Neurons derived from human embryonic stem cells extend long-distance axonal projections through growth along host white matter tracts after intra-cerebral transplantation

Mark Denham[1,2†], **Clare L. Parish**[1,2†], **Bryan Leaw**[1,2], **Jordan Wright**[1,2], **Christopher A. Reid**[1,2], **Steven Petrou**[1,2], **Mirella Dottori**[1] and **Lachlan H. Thompson**[1,2] *

[1] Centre for Neuroscience, University of Melbourne, Parkville, VIC, Australia

[2] Melbourne Brain Center, Florey Neuroscience Institute, University of Melbourne, Parkville, VIC, Australia

Human pluripotent stem cells have the capacity for directed differentiation into a wide variety of neuronal subtypes that may be useful for brain repair. While a substantial body of research has lead to a detailed understanding of the ability of neurons in fetal tissue grafts to structurally and functionally integrate after intra-cerebral transplantation, we are only just beginning to understand the *in vivo* properties of neurons derived from human pluripotent stem cells. Here we have utilized the human embryonic stem (ES) cell line *Envy*, which constitutively expresses green fluorescent protein (GFP), in order to study the *in vivo* properties of neurons derived from human ES cells. Rapid and efficient neural induction, followed by differentiation as neurospheres resulted in a GFP+ neural precursor population with traits of neuroepithelial and dorsal forebrain identity. Ten weeks after transplantation into neonatal rats, GFP+ fiber patterns revealed extensive axonal growth in the host brain, particularly along host white matter tracts, although innervation of adjacent nuclei was limited. The grafts were composed of a mix of neural cell types including differentiated neurons and glia, but also dividing neural progenitors and migrating neuroblasts, indicating an incomplete state of maturation at 10 weeks. This was reflected in patch-clamp recordings showing stereotypical properties appropriate for mature functional neurons, including the ability to generate action potentials, as well profiles consistent for more immature neurons. These findings illustrate the intrinsic capacity for neurons derived from human ES cells to integrate at a structural and functional level following transplantation.

Keywords: GFP, pluripotent, transplantation, regeneration, neural, electrophysiological, integration

INTRODUCTION

Substantial advances in pluripotent stem cell biology have fueled optimism for the development of stem cell-based procedures for brain repair. The concept of circuit reconstruction in the damaged brain through cell replacement has been pursued extensively in the Parkinson's disease (PD) field. Clinical trials using fetal donor tissue in PD patients have in fact provided proof-of-principle that new neurons, transplanted directly into the brain of the patient, can replace damaged circuitry with appropriate structural and functional features in order to significantly restore the disturbances in motor function associated with PD (Lindvall and Hagell, 2000; Lindvall and Bjorklund, 2004). Practical and ethical limitations associated with the use of fetal tissue as donor material has placed a significant emphasis on stem cells as a potentially superior cell source.

In the context of brain repair, pluripotent stem cells possess attractive features including a capacity for large-scale expansion as a cell source for neural transplantation procedures and potential for differentiation into a range of potentially therapeutic cell types relevant for specific neurological conditions (Barberi et al., 2003).

The rational development of stem cell-based transplantation procedures for brain repair requires a detailed understanding of the *in vivo* properties of stem cell-derived neurons, including their capacity for structural and functional incorporation into host circuitry.

Transplantation studies using fetal donor tissue from transgenic reporter mice have provided valuable insight into the growth properties of transplanted neurons in the host brain, including the important relationship between target connectivity and functional impact in certain cases (for review see Thompson et al., 2009; Gaillard and Jaber, 2011). The growth and connectivity of neurons derived from pluripotent stem cells have been less extensively explored in neural transplantation studies, with the exception of two recent studies using preparations generated from mouse embryonic stem (ES) cells grafted into neonatal mice (Ideguchi et al., 2010) and human ES cells grafted into adult athymic mice or immunosuppressed rats (Steinbeck et al., 2012).

Here we have made use of the human ES cell line *Envy*, which constitutively expresses green fluorescent protein (GFP) under the human β-actin promoter (Costa et al., 2005), in

order to more rigorously investigate the integration properties of neurons generated from human ES cells after transplantation into the neonatal rat brain. The GFP provided a useful surrogate marker of grafted tissue against which to measure important parameters such as graft volume and cellular composition. Importantly, immunohistochemical detection of GFP using the chromogen 3,3′-diaminobenzidine (DAB) combined with darkfield microscopy allowed for the mapping of graft-derived patterns of long-distance fiber growth from transplanted human ES cell-derived neurons at an unprecedented level of detail. The results show that grafted neurons are capable of extending long-distance projections within the host brain, particularly along white matter tracts of the internal and external capsules. At a functional level, the grafted neurons also displayed stereotypical electrophysiological properties and evidence of synaptic integration.

MATERIALS AND METHODS

hESC CULTURE

The ENVY-HES-3 cell line (BioTime) was cultured as previously described (Reubinoff et al., 2000; Conley et al., 2005). Briefly, hESCs were grown on mitomycin-C treated mouse embryonic fibroblasts (MEFs) in hESC medium consisting of high-glucose Dulbecco's modified Eagle's medium (DMEM) without sodium pyruvate, supplemented with 1% insulin/transferrin/selenium, 0.1 mM β-mercaptoethanol, 1% non-essential amino acids (NEAA), 2 mM glutamine, 25 U/ml penicillin, 25 μg/ml streptomycin (all from Invitrogen), and 20% fetal calf serum (Hyclone) or on mitomycin-C treated human foreskin fibroblasts (HFF) in knockout serum replacement (KSR) media consisting of DMEM/nutrient mixture F-12, supplemented with 0.1 mM β-mercaptoethanol, 1% NEAA, 2 mM glutamine, 25 U/ml penicillin, 25 μg/ml streptomycin, and 20% KSR (all from Invitrogen). All cells were cultured at 37°C 5% CO_2. Colonies were mechanically dissected every 7 days and transferred to freshly prepared MEFs or HFFs. Media was changed every second day.

PA6 NEURAL INDUCTION

hESCs were mechanically dissected into pieces approximately 0.5 mm in diameter and transferred to an organ culture plate of PA6 cells (Riken) in co-culture medium containing Glasgow minimum essential medium, supplemented with 8% KSR, 1% NEAA, 2 mM L-glutamine, 1 mM sodium pyruvate, β-mercaptoethanol 0.1 mM, penicillin 25 U/ml, streptomycin 25 μg/ml. Cells were differentiated on PA6 stromal cells for 10 days with Noggin (500 ng/ml, R&D systems) added to the media for the first 4 days. Following PA6 co-culture neural rosettes were dissected into 0.5-mm fragments and further cultured as neurospheres in suspension in low-attachment 96-well plates (Corning) in N2B27 medium containing a 1:1 mix of neurobasal medium with DMEM: nutrient mixture F-12 medium, supplemented with 1% insulin/transferrin/selenium, 1% N2, 1% B27, 0.3% glucose, 25 U/ml penicillin, and 25 μg/ml streptomycin (all from Invitrogen), with basic fibroblast growth factor (bFGF) and epidermal growth factor (EGF; 20 ng/ml each, R&D systems). After 7 days in suspension, neurospheres were dissociated into single cells with triple express medium (Invitrogen) and re-suspended

at 100,000 cells/μl for transplantation in HBSS without Ca^{2+} or Mg^{2+} supplemented with 0.05% DNase. The 7-day differentiation period was chosen based on the onset of neuronal differentiation, where the first detectable βIII-tubulin+ cells appear around 5–7 days.

ANIMALS AND TRANSPLANTATION

The use of animals in this study conformed to the Australian National Health and Medical Research Council's published Code of Practice for the Use of Animals in Research, and experiments were approved by the Florey Neuroscience Institutes Animal Ethics Committee (#09-036).

All surgical procedures were performed using a Cunningham (Stoelting, Germany) adaptor fitted to a stereotaxic frame (Kopf, Germany). A total of 20 neonatal (postnatal day 2) Sprague Dawley rats were used as transplant recipients. Hypothermic anesthesia was induced by placing each neonate in ice for 5 min and maintained by adding dry ice to absolute ethanol in the reservoir built into Cunningham adaptor stage. Under deep anesthesia, each rat received an injection of 1×10^5 cells in a volume of 1 μl using a glass cannula fitted to a 5-μl microsyringe (SGE Analytical Sciences, Australia) according to a microtransplantation approach described previously (Nikkhah et al., 2000). Cells were injected into the right striatum (0.7 mm anterior and 1.9 mm lateral to bregma, 2.9 mm below the dura) over 1 min and the cannula was left in place a further 2 min before withdrawal. The underdeveloped state of the immune system in neonatal animals avoids the need for immunosuppressive treatment in intra-cerebral xeno-grafting studies. The survival time for these animals was 10 weeks. Fourteen animals were processed for histological analysis and six animals were used for electrophysiological studies.

TISSUE PREPARATION AND IMMUNOHISTOCHEMISTRY

Ten weeks after transplantation, 14 animals received a lethal dose of pentobarbitone and were trans-cordially perfused with 50 ml saline (0.9% w/v) followed by 200–250 ml paraformaldehyde (PFA; 4% w/v in 0.1 M PBS). The brains were removed, post-fixed a further 2 h in PFA and cryo-protected in sucrose (25% w/v in 0.1 M PBS). Brains were sectioned in the coronal, sagittal, or horizontal plane in 12 series at a thickness of 30 μm on a freezing microtome (Leica, Germany).

Immunohistochemical procedures were performed as previously described (Thompson et al., 2005). Free-floating sections were incubated overnight at room temperature with primary antibodies diluted in 0.1 M PBS containing 5% normal serum and 0.25% Triton X-100 (Ameresco, USA). Secondary antibodies diluted in PBS with Triton X-100 and 2% normal serum were applied for 2 h at room temperature. The primary–secondary antibody complex was visualized by peroxidase driven precipitation of DAB or conjugation of a fluorophore. Fluorescent slide mounted sections were cover-slipped with fluorescent mounting medium (DAKO, USA). DAB-labeled sections were dehydrated in alcohol and xylene and cover-slipped with DePex mounting medium (BDH Chemicals, UK). For counterstaining of cell nuclei, slide mounted tissue was incubated with 4,6-diamino-2-phenylindole (DAPI, 1:1000; Sigma) for 5 min prior to cover-slipping.

Primary antibodies and dilution factors were as follows: mouse anti-βIII-tubulin (1:500; Millipore), rat anti-Ctip2 (1:500; AbCam), rabbit anti-Cux1 (1:500; Santa Cruz Biotechnology), goat anti-doublecortin (1:400; Santa Cruz Biotechnology), rabbit anti-GFAP (1:200; DAKO), chicken anti-GFP (1:1000, AbCam), rabbit anti-GFP (1:20,000; AbCam), mouse anti-NeuN (1:200; Millipore), mouse anti-Oct4 (1:100; Santa Cruz Biotechnology), rabbit anti-Otx2 (1:4000; Millipore), rabbit anti-Olig2 (1:200; Millipore), mouse anti-Pax7 (1:80; DSHB), mouse anti-Pax6 (1:40; DSHB), mouse anti-PSA-NCAM (1:100; Santa Cruz Biotechnology), mouse anti-RIP (1:5000; Millipore) mouse anti-synaptophysin (1:200; Sigma), goat anti-Sox2 (1:100; R&D systems), and rabbit anti-TBR1 (1:1000; Millipore). For DAB-based detection of GFP, a biotinylated goat anti-rabbit secondary antibody (Vector Laboratories, USA) was subsequently conjugated with streptavidin-HRP using the Vectastain ABC Elite kit (Vector Laboratories, USA). For immunofluorescence, species-specific secondary antibodies generated in donkey and conjugated with the Dylight^{TM} range of fluorophores with various peak emission wavelengths including 488, 549, and 633 were used at a dilution of 1:500 (Jackson ImmunoResearch, USA).

IMAGING AND QUANTIFICATION

To provide macroscopic illustrations of GFP immunoreactivity, montages of single darkfield images captured using a 20× objective were constructed using a Leica DM6000 B upright light microscope equipped with a motorized stage. Graft area was calculated according to Cavalieri's principle (Cavalieri, 1966) by measuring the GFP+ graft area in every 12th DAB-stained tissue section ($n = 10$). Fluorescent images were captured using a Zeiss Meta laser scanning confocal upright microscope. The intensity and contrast of each image was enhanced through adjustment of the levels in individual color channels using Photoshop (Adobe). The cellular densities of the grafts were estimated through stereological assessment of DAPI-labeled nuclei in defined volumes within 5 of the larger grafts on an Olympus brightfield upright microscope equipped with Stereo Investigator software (Microbrightfield). The percentage of neurons was estimated through quantification of the overlap between DAPI and NeuN within the GFP+ graft area (>500 cells counted; $n = 4$).

ELECTROPHYSIOLOGY

Ten weeks following implantation rats were anesthetized with 1–2% isoflurane before decapitation. Brain slices (300 μm thick) cut using a vibratome in the coronal plane were prepared in a saline ice bath and kept at room temperature until recording. The slices were transferred to a recording chamber constantly perfused with artificial CSF solution at 34°C consisting of (in mM): 125 NaCl, 2.5 KCl, 25 NaHCO$_3$, 1.25 NaH$_2$PO$_4$, 1 MgCl$_2$, 2 CaCl$_2$, and 10 Glucose, aerated with 95% O$_2$ and 5% CO$_2$ to a final pH of 7.4. Whole-cell patch-clamp recordings were made using a MultiClamp 700A amplifier and pClamp acquisition software (Molecular Devices, Sunnyvale, CA, USA) from explants unambiguous identified by visualizing GFP, detected under standard epifluorescence before switching to infrared DIC imaging (BX51, Olympus). Electrodes were pulled using a Sutter P-2000

puller (Sutter Instruments, Novato, CA, USA) from borosilicate micropipettes (World Precision Instruments, Sarasota, FL, USA) with an initial resistance of around 3–6 MΩ. The electrodes were filled with intracellular solution consisting of (in mM): 125 KGlu, 4 KCl, 2 MgCl$_2$, 10 HEPES, 10 EGTA, 4 ATP-Mg, and 0.3 GTP-Na, and 8 biocytin hydrochloride at a final pH of 7.3. D-Mannitol was used to adjust osmolarity to 300 mOsm. Standard capacitance compensation and bridge balance techniques were employed. Average membrane resistance was 427 ± 127 MΩ and average cell capacitance was 65 ± 19 pF for all recordings. Voltage recordings were digitized at ~83 kHz and filtered *post hoc* using a 6-kHz Bessel low-pass filter. Experiments were completed at room temperature (20–22°C). A holding current was injected into neurons if required setting their holding potential to −65 mV. A current injection/action potential frequency relationship was established by injecting progressively more depolarizing current steps of 400 ms duration (20 pA incremental steps from −100 to 280 pA) with 300 ms baseline recording on either side of the step. A gap of 500 ms was used between each sweep.

RESULTS

RAPID CONVERSION OF GFP-EXPRESSING HUMAN ES CELLS TO NEURAL LINEAGE WITH REGIONAL FEATURES

In this study we made use of a human ES cell line ubiquitously expressing GFP under the human β-actin (ACTB) promoter. The cells were prepared for transplantation through neural induction on stromal cells (PA6) with noggin for 10 days, followed by partial differentiation as neurospheres for a further 7 days. Immunocytochemical analysis of thin (10 μm) sections through individual neurospheres showed robust, cytoplasmic distribution of GFP in all cells (**Figures 1A–C**). The spheres were rich in cells expressing markers consistent with an early neuroepithelial identity, including Pax6 and Sox2 (**Figures 1H–J**), and also appeared to have some level of spatial organization based on the heterogeneous distribution of these markers and the consistent appearance of rosette-like structures (**Figures 1H–K**). Complete lack of expression of Oct4 suggested efficient neural induction without the persistence of a residual pluripotent stem cell population (**Figures 1D–G**). Cells in the periphery of the spheres had begun to acquire neuronal features, including expression of the neurofilament protein βIII-tubulin and basic neuronal morphology (**Figures 1L–O**). We also observed the expression of transcription factors that define regional organization during normal embryogenesis, including Otx2, which is expressed in the developing telencephalon, as well as the dorsal marker, Pax7 (**Figure 2**).

SIZE AND COMPOSITION OF HUMAN ES CELL GRAFTS

Ten weeks after transplantation, immunohistochemistry for GFP revealed surviving grafts in 10 out of 14 animals. The grafts presented as discrete deposits with dense GFP+ cores (**Figure 3A**). The size of the grafts varied considerably (0.09–2.91 mm^3) with an average volume of 0.79 ± 0.88 mm^3. Most of the grafts were well placed in the head of the striatum (**Figure 3A**), although in two animals the majority of the grafted cells were found in the overlying cortex (**Figure 3A**) – likely due to backflow up the needle tract – and in another two animals small grafts were found in the corpus callosum. Inspection of DAPI-labeled
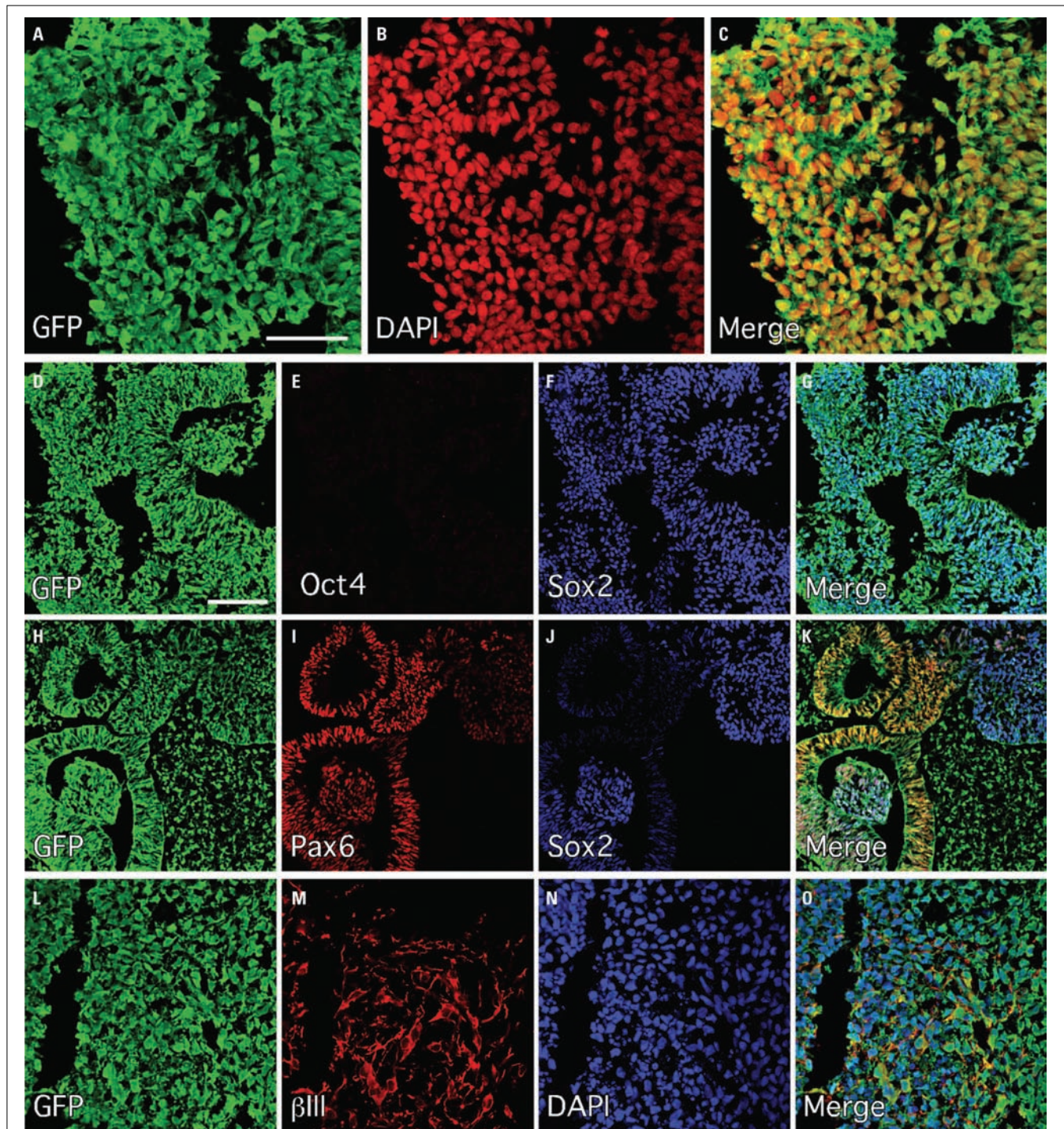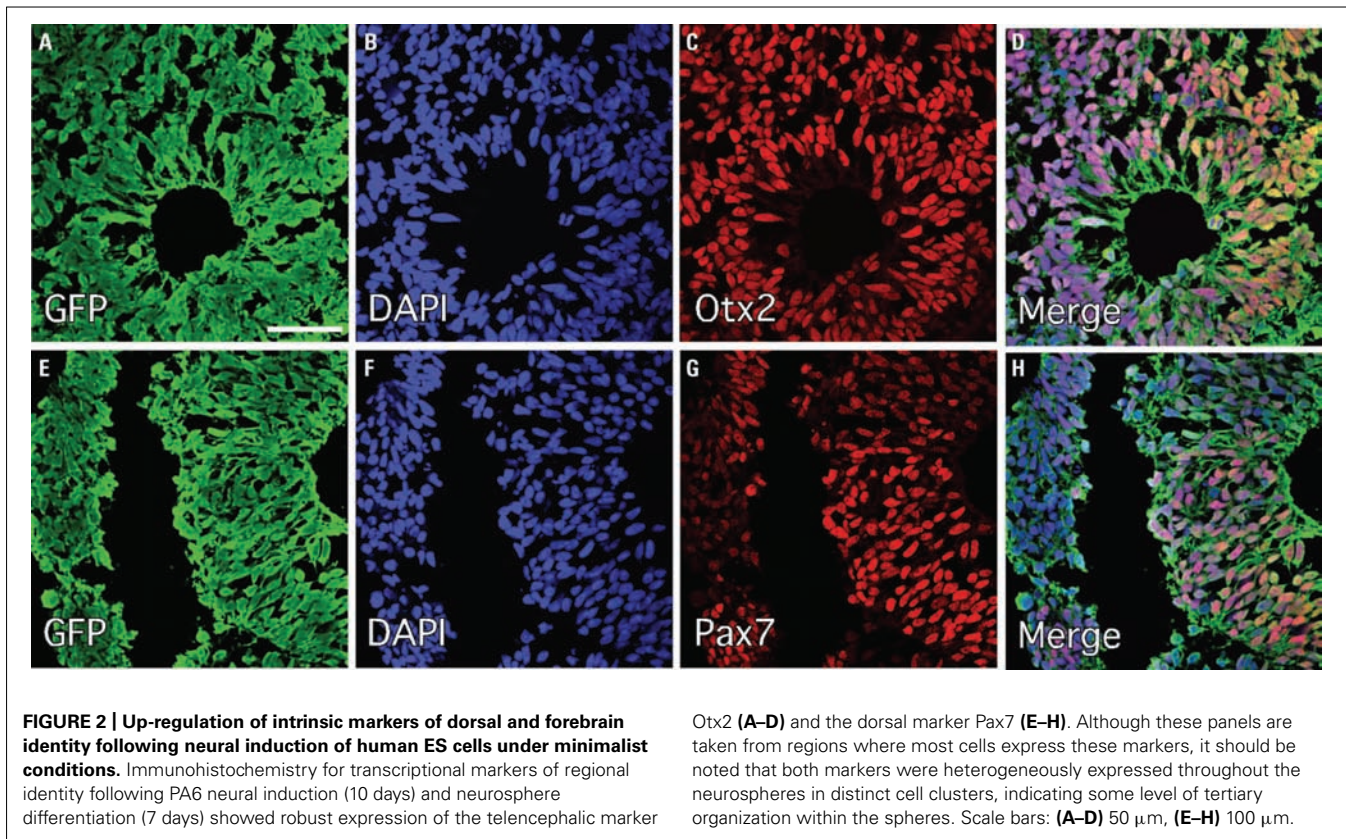
FIGURE 1 | Efficient neural induction of the human ES cell line Envy as assessed by immunohistochemistry following 10 days on PA6 and 7 days differentiation as neurospheres. (A–C) GFP (green) was robustly expressed in all cells (DAPI; red). **(D–G)** Sox2 (blue) was expressed widely and Oct4 (red) was uniformly down-regulated throughout all cultures. **(H–K)** Pax6 (red) was also widely expressed throughout the cultures and largely overlapped with Sox2 expression domains including prominent expression in neural rosette structures. **(L–O)** These panels are show a region in the periphery of the differentiating neurospheres where βIII-tubulin (red) was expressed in cells with neuronal morphology. Scale bars: **(A–C)** 50 μm, **(D–O)** 100 μm.

nuclei within the grafts showed that the cellular distribution was quite homogeneous (**Figure 4A**) with an average density of $2.46 \pm 0.40 \times 10^5$ cells/mm^3. When applying this across the different graft volumes the average number of surviving cells was approximately $2.14 \pm 2.20 \times 10^5$ (i.e., approximately twice the 1×10^5 cells originally grafted) suggesting substantial growth of

FIGURE 2 | Up-regulation of intrinsic markers of dorsal and forebrain identity following neural induction of human ES cells under minimalist conditions. Immunohistochemistry for transcriptional markers of regional identity following PA6 neural induction (10 days) and neurosphere differentiation (7 days) showed robust expression of the telencephalic marker Otx2 **(A–D)** and the dorsal marker Pax7 **(E–H)**. Although these panels are taken from regions where most cells express these markers, it should be noted that both markers were heterogeneously expressed throughout the neurospheres in distinct cell clusters, indicating some level of tertiary organization within the spheres. Scale bars: **(A–D)** 50 μm, **(E–H)** 100 μm.

the graft after transplantation. Immunohistochemistry for Ki67 showed the persistence of a small population of dividing cells within the graft at 10 weeks (**Figure 4C**). The majority of the Ki67+ cells also expressed the neural progenitor marker Sox2 (**Figure 4C**). We did not observe any gross morphological features suggesting aggressive cell division indicative of tumor formation.
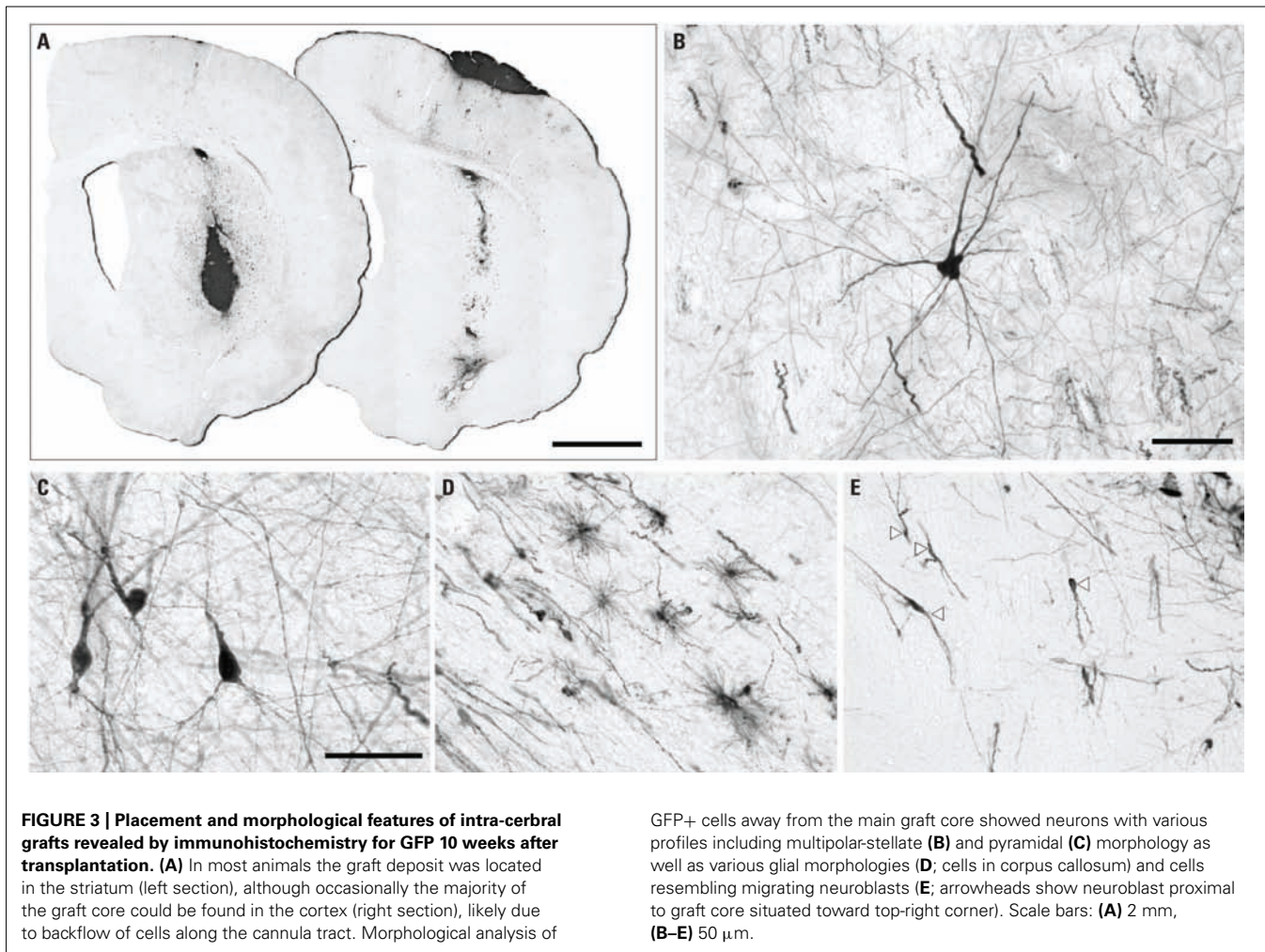
In addition to the dense graft cores, clusters of sparsely distributed GFP+ cells could be found in the adjacent host parenchyma, thus allowing for an assessment of cell morphology. The results showed morphological profiles consistent with various neural cell types including immature, migrating neuroblasts as well as terminally differentiated neurons and glia (**Figures 3B–E**). Immunohistochemistry for GFP along with markers indicative of cell phenotype confirmed the presence of multiple neural cell types within the grafts. The grafts were rich in migrating neuroblasts based on staining for PSA-NCAM and doublecortin (Dcx) and these cells were often seen emanating from the graft core into the surrounding host parenchyma (**Figure 4B**) and clustered in nearby striatal fiber bundles (not shown). The grafts also contained cells with mature neuronal and glial features based on labeling for neuronal nuclei (NeuN) as well as the glial markers GFAP, Olig2, and RIP (**Figure 4**). The neuronal nuclei protein is a ubiquitous marker for terminally differentiated neurons and as such gives a reasonable indication of the total neuronal contribution within the grafted tissue. Quantification of NeuN+ cell numbers as a fraction of DAPI+ cells within sections of GFP+ tissue showed that the average contribution of neurons was $56.73 \pm 9.24\%$ ($n = 5$). Based on the average cell density and graft volume, this equates

to an average of $1.20 \pm 1.27 \times 10^5$ neurons per graft. Glia with characteristics of either astrocytes or oligodendrocytes were also found in the grafts, although more sparsely distributed than the NeuN+ cells. We did not detect cells expressing the pluripotent marker Oct4 or the neuroepithelial marker Pax6 in any of the grafted animals (not shown).

Based on results showing a dorsal forebrain identity of partially differentiated cells *in vitro* (**Figure 2**), we looked for expression of markers typical for cortical neurons within the grafts. The T-box transcription factor, Tbr1, which is widely expressed through all layers of the mature rodent cortex was scattered sparsely throughout the grafts (**Figures 5F–H**). We also looked at expression of transcription factors known to differentiate between different cortical layers within the fully developed cortex, including Cux1 and Ctip2, which are expressed in superficial and deeper layers respectively (**Figure 5A**). Distinct clusters of Ctip2+ cells could be found in the GFP+ grafts, while virtually no Cux1+ cells were detected (**Figures 5B–E**). This was the case for grafts located in either the striatum or cortex.

LONG-DISTANCE AXONAL GROWTH ALONG HOST WHITE MATTER TRACTS AFTER TRANSPLANTATION OF NEURALIZED HUMAN ES CELLS

A striking feature of the transplants was the extensive degree of GFP+ fiber outgrowth over long distances within the host brain. The general pattern of growth was remarkably consistent across the different cases, including animals with either striatal or cortical graft placement, although the overall degree of growth appeared

FIGURE 3 | Placement and morphological features of intra-cerebral grafts revealed by immunohistochemistry for GFP 10 weeks after transplantation. (A) In most animals the graft deposit was located in the striatum (left section), although occasionally the majority of the graft core could be found in the cortex (right section), likely due to backflow of cells along the cannula tract. Morphological analysis of GFP+ cells away from the main graft core showed neurons with various profiles including multipolar-stellate **(B)** and pyramidal **(C)** morphology as well as various glial morphologies **(D**; cells in corpus callosum) and cells resembling migrating neuroblasts **(E**; arrowheads show neuroblast proximal to graft core situated toward top-right corner). Scale bars: **(A)** 2 mm, **(B–E)** 50 μm.

more extensive in animals with larger grafts. The GFP+ fibers could be visualized in fine detail under darkfield microscopy as illustrated in representative sections from three brains cut in various section planes (**Figure 6**, A high resolution version of this figure can be found online at: http://www.frontiersin.org/files/images/23963/darkfield_overview.jpg).

At the graft site, fibers could be seen emanating from the graft and extending into the striatal parenchyma and ventrally into sub-striatal nuclei including the ventral palladium (**Figure 7A**). Another prominent feature within the striatum was the presence of polarized groups of fibers clustered within striatal fiber bundles (**Figures 6 and 7K**). The association of GFP+ fibers with host white matter tracts was a definitive feature of the long-distance axonal outgrowth from grafted neurons. Coronal and horizontal sections showed that GFP+ fibers extended throughout the external capsule of both hemispheres and exited into adjacent cortical regions at all rostro-caudal levels examined, including: somatosensory and insular cortical areas at rostral levels (**Figure 6**) and perirhinal and entorhinal areas at more caudal levels (**Figure 7G**). Graft-derived fibers also exited the corpus callosum dorsally through the cingulum to innervate the overlying cingulate cortex and ventrally at the midline to innervate the septum (**Figures 7C,I**). Anterior to the graft there was a robust outgrowth of GFP+ fibers extending through forceps minor into the adjacent anterior regions of cortex including the secondary motor, cingulate, and pre-limbic areas (**Figures 7B,C**). Caudal to the graft there was a substantial outgrowth that followed the internal capsule, along striatal fiber bundles (**Figures 6 and 7K**), through the entopeduncular nucleus (**Figure 7E**) and into the ventral midbrain where most fibers were associated with myelinated fiber bundles within the substantia nigra pars reticulata and also traversed through the underlying cerebral peduncle (**Figure 7F**). Many fibers also left the internal capsule and coursed lateral into the amygdala and medial to innervate adjacent nuclei including the zona incerta, and surrounding Forel's fields, as well as deeper thalamic nuclei (**Figure 7H**) and the underlying hypothalamus. Further caudal, GFP+ fibers were found in the periaqueductal gray, deep mesencephalic nuclei and white matter tracts immediately dorsal to the pontine nuclei. Analysis of horizontal sections showed that GFP+ fibers extended well beyond the midbrain and into the brainstem (**Figures 6 and 7L**). Although the GFP+ extended from white matter tracts into adjacent host nuclei, including the striatum, cortex, thalamus, septum, the prevailing morphological features were consistent with elongated *en passant* fibers rather
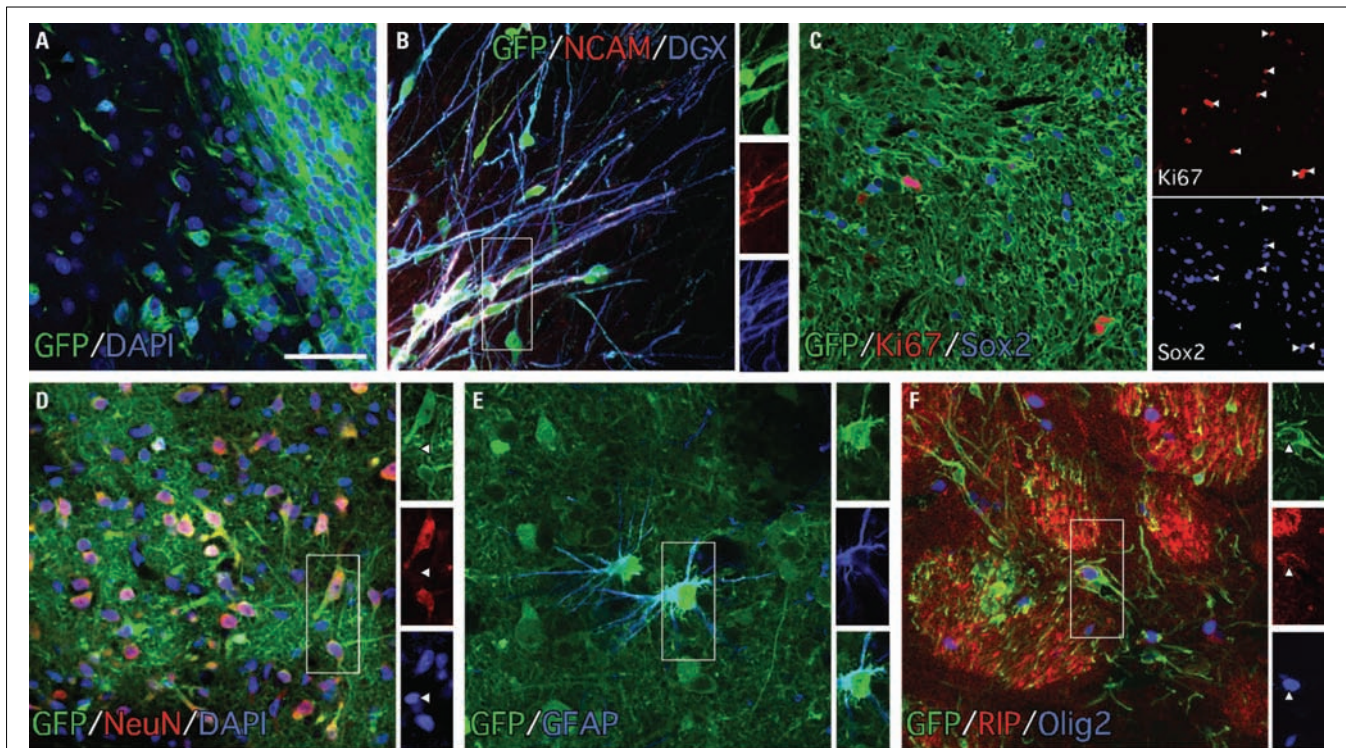
FIGURE 4 | The grafts were composed of immature and differentiated neural cell types as revealed by immunochemistry for GFP and phenotypic markers 10 weeks after transplantation. (A) Staining for DAPI (blue) and GFP (green) shows the densely packed graft core at the periphery of the graft within the GFP− host tissue. **(B)** Many of the cells with migrating neuroblast morphology expressed both doublecortin (blue) and PSA-NCAM (red; boxed area enlarged as single color channels). **(C)** The grafts contained a population of dividing (Ki67+, red) cells 10 weeks after transplantation and many of the Ki67+ cells also expressed the neural marker Sox2+ (blue; arrowheads show overlap in single color channels). **(D)** The grafts were rich in differentiated neurons (>50%) based on immunohistochemistry for NeuN (red; arrowheads in single color channels highlight the relatively smaller nuclear size of NeuN− cells, which are likely glia). Immunohistochemistry for glial markers showed that the grafts also contained smaller populations of differentiated astrocytes (**E**; GFAP+, blue) and myelinating oligodendrocytes (**F**; RIP+/Olig+). Scale bars: **(A–F)** 50 μm.
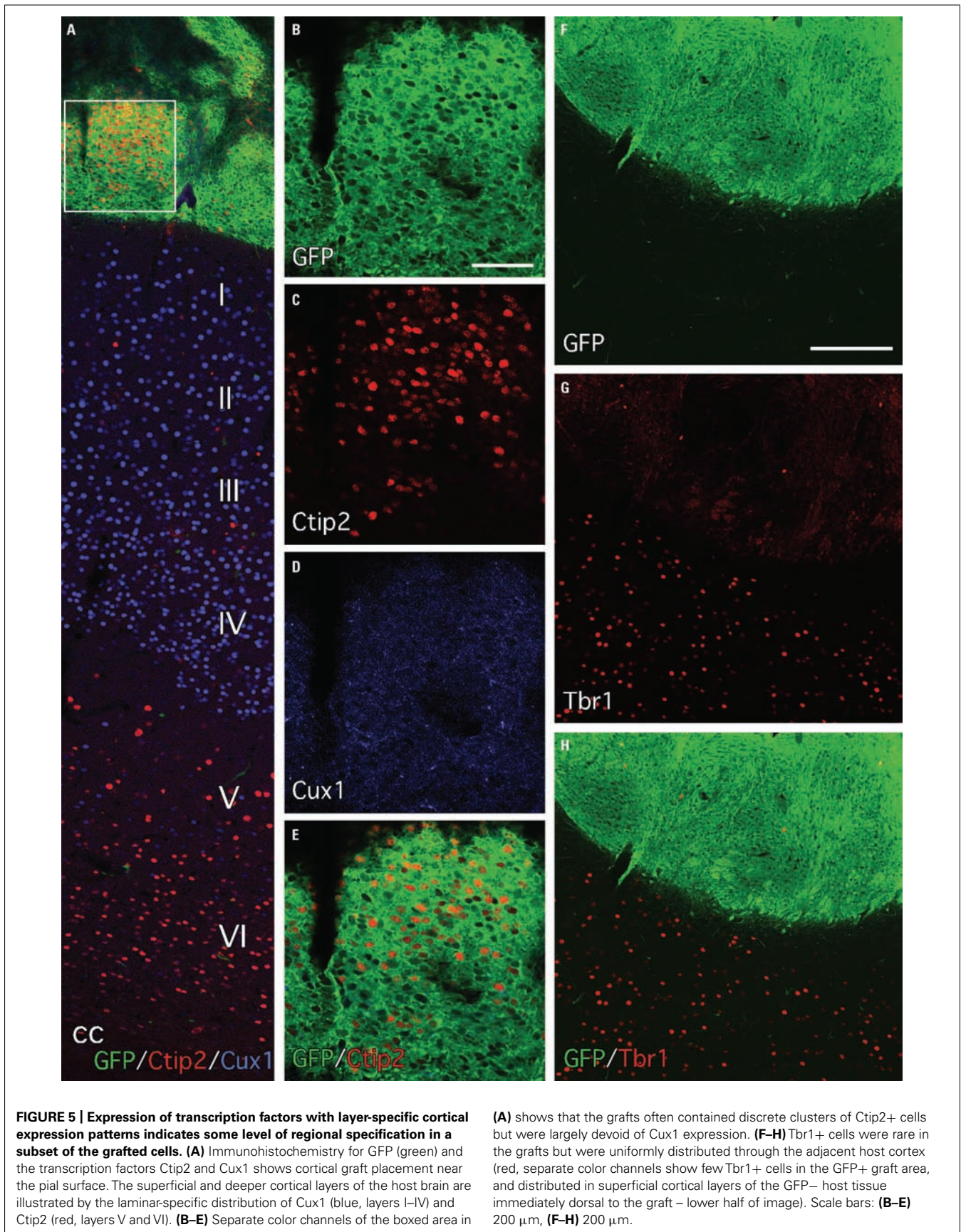
than elaborated patterns of terminal arborization in these areas (**Figure 7**).
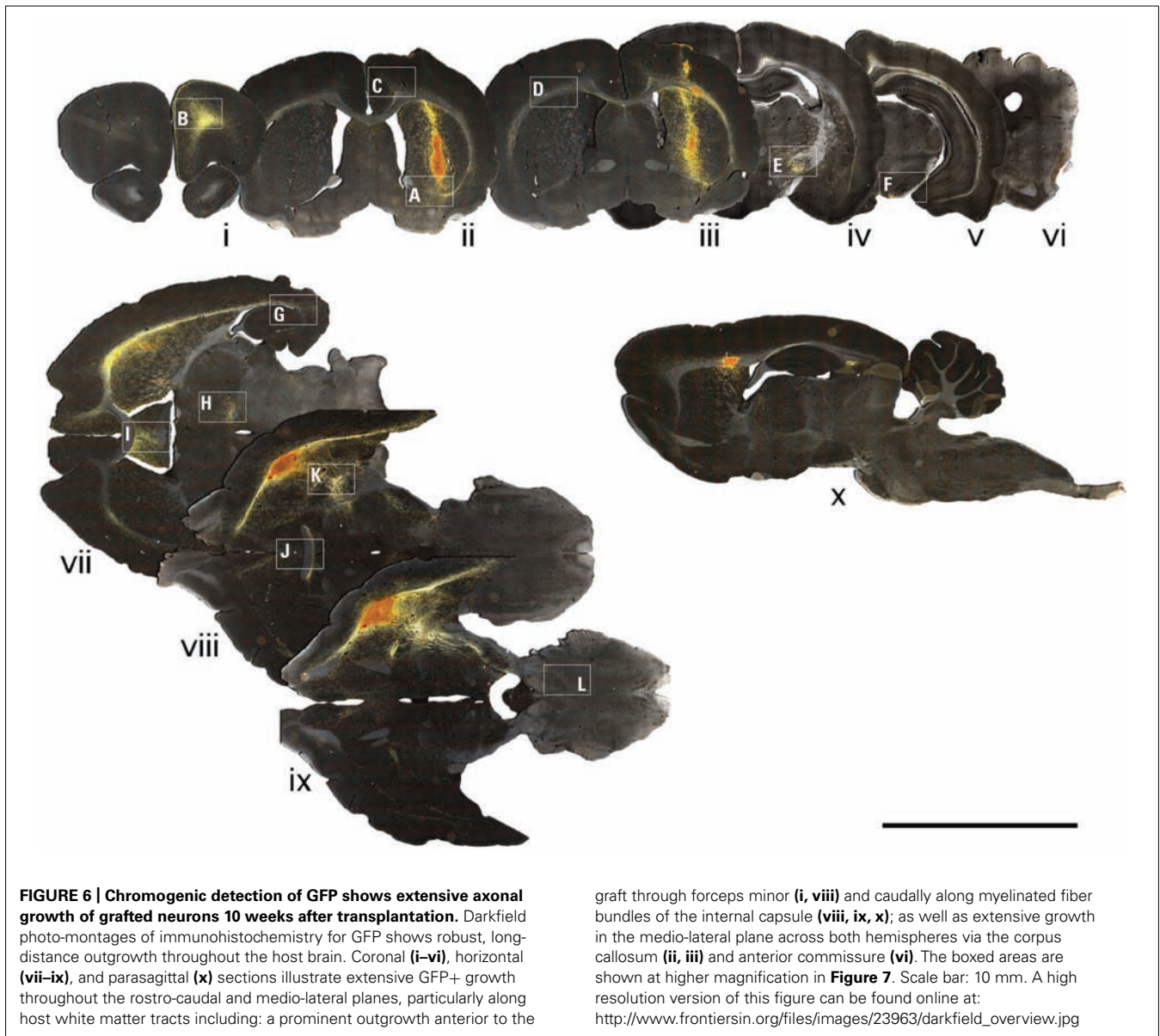
Immunohistochemistry for the myelin-associated protein RIP highlighted the growth along host white matter tracts as a distinctive feature of graft-derived axonal outgrowth. This was seen throughout nearly all major myelinated pathways forming the internal and external capsules, and was particularly prominent along the striatal fiber bundles near the graft site (**Figures 8A–E**) and throughout the anterior commissure (**Figures 8F–H**). The striatal or cortical placement did not appear to impact on the general pattern of fiber outgrowth, however there was noticeably more outgrowth caudal to the graft along striatal fiber bundles and into the midbrain and brainstem in animals where the graft was placed in the striatum and especially where small graft deposits were found in the corpus callosum (e.g., see the extensive outgrowth in horizontal sections in **Figure 6**).

TRANSPLANTED HUMAN ES CELL-DERIVED NEURONS DISPLAY STEREOTYPICAL ELECTROPHYSIOLOGICAL PROPERTIES *EX VIVO*

Ten weeks following transplantation brain slices were prepared from six rats for whole-cell patch-clamp recording. The GFP expression allowed for the unambiguous identification of transplanted cells within the slice preparation. In three of the six animals

GFP expression was clearly observed with a total of four cells in three intra-striatal grafts successfully recorded from. *Post hoc* processing for biocytin demonstrated co-localization with GFP confirming that all cells recorded from originated from the graft. These cells had morphology consistent with that expected for a neuron (**Figure 9A**) and active properties that are consistent with a neuronal phenotype. The major electrophysiological phenotype observed in GFP+ cells was the ability to generate action potentials with membrane depolarization. Two of four cells showed a typical input–output curve with increasing action potential firing frequency seen with increasing stimulating current (**Figure 9C**). In the other two neurons action potentials were observed but the maximum firing rate seen was much lower which is typically seen in immature neurons. At resting membrane potential excitatory post-synaptic potentials were observed and depolarized the neurons sufficiently to evoke a spontaneous action potential in two of the four cells recorded (**Figure 9D**). In summary, the grafted cells displayed appropriate functional properties for integrated neurons. We also looked for histological evidence of synaptic afferent input to the transplanted neurons through immunohistochemistry for synaptophysin. The GFP+ grafts were rich in synaptophysin+ terminals both throughout the periphery of the graft and also deep within the graft core. Thin (∼5 μm) optical

FIGURE 5 | Expression of transcription factors with layer-specific cortical expression patterns indicates some level of regional specification in a subset of the grafted cells. (A) Immunohistochemistry for GFP (green) and the transcription factors Ctip2 and Cux1 shows cortical graft placement near the pial surface. The superficial and deeper cortical layers of the host brain are illustrated by the laminar-specific distribution of Cux1 (blue, layers I–IV) and Ctip2 (red, layers V and VI). **(B–E)** Separate color channels of the boxed area in

(A) shows that the grafts often contained discrete clusters of Ctip2+ cells but were largely devoid of Cux1 expression. **(F–H)** Tbr1+ cells were rare in the grafts but were uniformly distributed through the adjacent host cortex (red, separate color channels show few Tbr1+ cells in the GFP+ graft area, and distributed in superficial cortical layers of the GFP− host tissue immediately dorsal to the graft – lower half of image). Scale bars: **(B–E)** 200 μm, **(F–H)** 200 μm.

FIGURE 6 | Chromogenic detection of GFP shows extensive axonal growth of grafted neurons 10 weeks after transplantation. Darkfield photo-montages of immunohistochemistry for GFP shows robust, long-distance outgrowth throughout the host brain. Coronal **(i–vi)**, horizontal **(vii–ix)**, and parasagittal **(x)** sections illustrate extensive GFP+ growth throughout the rostro-caudal and medio-lateral planes, particularly along host white matter tracts including: a prominent outgrowth anterior to the graft through forceps minor **(i, viii)** and caudally along myelinated fiber bundles of the internal capsule **(viii, ix, x)**; as well as extensive growth in the medio-lateral plane across both hemispheres via the corpus callosum **(ii, iii)** and anterior commissure **(vi)**. The boxed areas are shown at higher magnification in **Figure 7**. Scale bar: 10 mm. A high resolution version of this figure can be found online at: http://www.frontiersin.org/files/images/23963/darkfield_overview.jpg

sections through the graft cores allowed us to resolve for individual GFP+ cells and showed the localization of synaptophysin at the lipid membrane in some cells (**Figure 9B**). Interestingly, some of the synaptophysin+ domains appeared to be GFP-negative (**Figure 9B**) suggesting afferent input of host origin.

DISCUSSION

Although there has been a significant period of rapid progress in the pluripotent stem cell field over the last decade, the success we have seen in the culture dish, allowing for the procurement of a diverse range of neuronal phenotypes from highly expandable stem cell populations, has been difficult to translate into an *in vivo* setting with effective and predictable outcomes in animal models of brain injury. The rational development of stem cell-based procedures for brain repair will ultimately be built on a detailed understanding of the properties of stem cell-derived cell preparations after transplantation. Here we have generated detailed information on the composition and integration properties of neural cell preparations generated from a human ES cell line ubiquitously expressing GFP.

Traditional protocols for neural induction describe extended *in vitro* culturing periods for the induction and expansion of neural progenitors, derived from human ES cells (Reubinoff et al., 2001; Perrier et al., 2004; Tabar et al., 2005; Sonntag et al., 2007). More recently, shorter and more efficient neural induction protocols have been reported using small molecules (Chambers et al., 2009; Li et al., 2011; Morizane et al., 2011). We also describe here a shortened induction and expansion protocol for generating neural progenitors by combining noggin application with growth on PA6 stromal cells. Previous studies have shown that antagonism of BMP signaling with noggin significantly improves the efficiency of neural induction of human ES cells while concomitantly
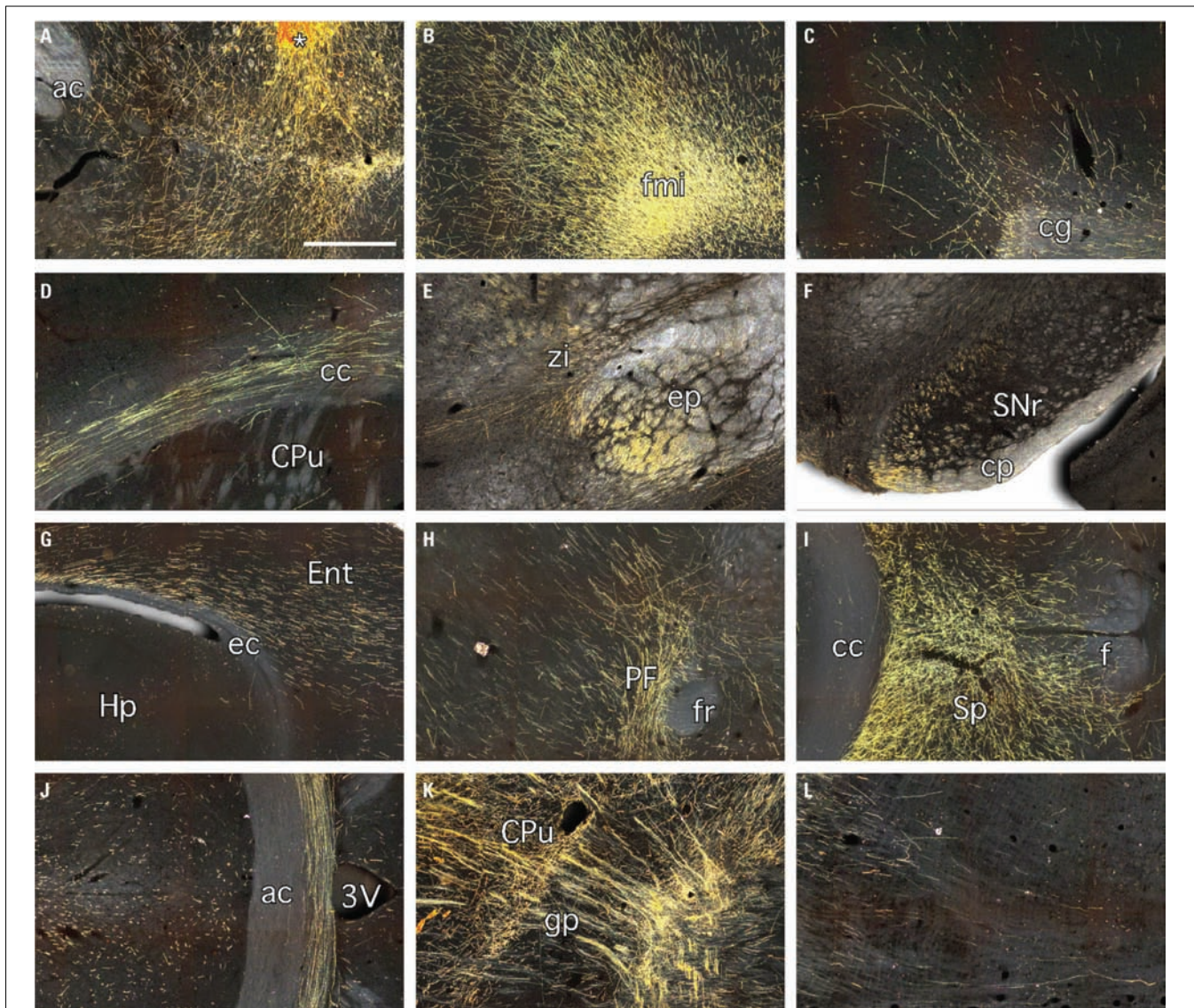
FIGURE 7 | Darkfield images of immunohistochemistry for GFP 10 weeks after grafting of neural cell preparations generated from human ES cells. These panels are enlarged versions of the boxed areas depicted in **Figure 6** and show GFP+ fibers: **(A)** extending from the graft core (*) into the surrounding striatum and ventrally into the ventral palladium; **(B)** coursing through forceps minor and into the adjacent secondary motor, cingulate, and pre-limbic cortices; **(C)** extending through the cingulum into the overlying cingulate cortex; **(D)** extending through the corpus callosum of the contralateral hemisphere; **(E)** running caudally through the entopeduncular nucleus and branching medially into the adjacent zona incerta and nearby thalamic nuclei; **(F)** at the level of the midbrain, predominately associated with white matter tracts in the substantia nigra pars reticulata and the underlying cerebral peduncle; **(G)** exiting the caudal and ventral extremities of the external capsule into the adjacent entorhinal cortex; **(H)** at the level of the parafascicular thalamic nucleus; **(I)** in the septum; **(J)** running through the anterior commissure at the midline; **(K)** extending along myelinated fiber bundles of the internal capsule and; **(L)** in the brain stem. 3V, 3rd ventricle; ac, anterior commissure; cc, corpus callosum; cg, cingulum; cp, cerebral peduncle; CPu, caudate putamen; ec, external capsule; Ent, entorhinal cortex; ep, entopeduncular nucleus; f, fornix; fmi, forceps minor; fr, fasciculus retroflexus; gp, globus pallidus; Hp, hippocampus; PF, parafascicular nucleus; SNr, substantia nigra pars reticulata; Sp, septum; zi, zona incerta. Scale bar: **(A–L)** 500 μm.

suppressing differentiation into extra-embryonic endoderm (Pera et al., 2004; Dottori and Pera, 2008). The absence of pluripotency markers *in vitro*, such as Oct4, and up-regulation of early neural (Sox2, Pax6) and neuronal (βIII-tubulin) markers shows that expanding human ES cells can be efficiently converted into neural precursors capable of neuronal differentiation over a relatively short timeframe. This was reflected in the resulting grafts, which were composed of mixed neural cell types and did not contain Oct4+ cells. Furthermore, lack of Pax6+ cells in the grafts suggests the cells had continued to differentiate *in vivo* beyond an early neuroepithelial state.

Unambiguous detection of grafted tissue in the host brain through GFP expression allowed us to determine key features of graft size and composition. The average size and density of
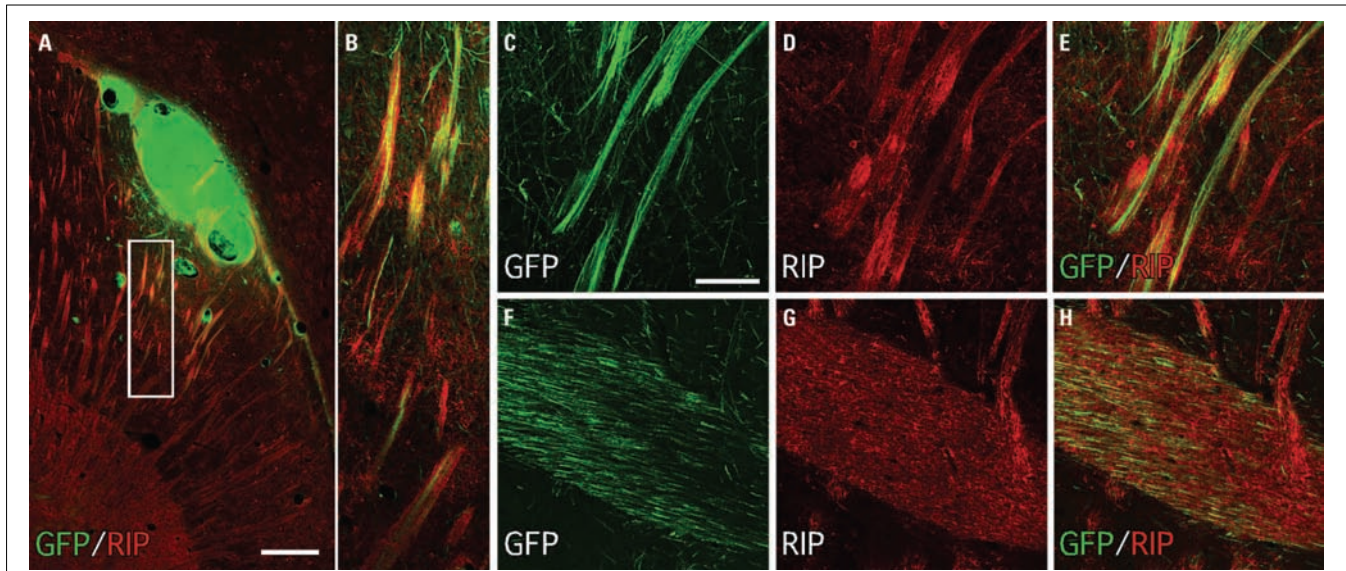
FIGURE 8 | Immunohistochemistry for the oligodendrocyte protein RIP (CNPase) highlights the association of GFP+ fibers from transplanted human ES cell-derived neurons with host myelinated fiber bundles. (A,B) A low-power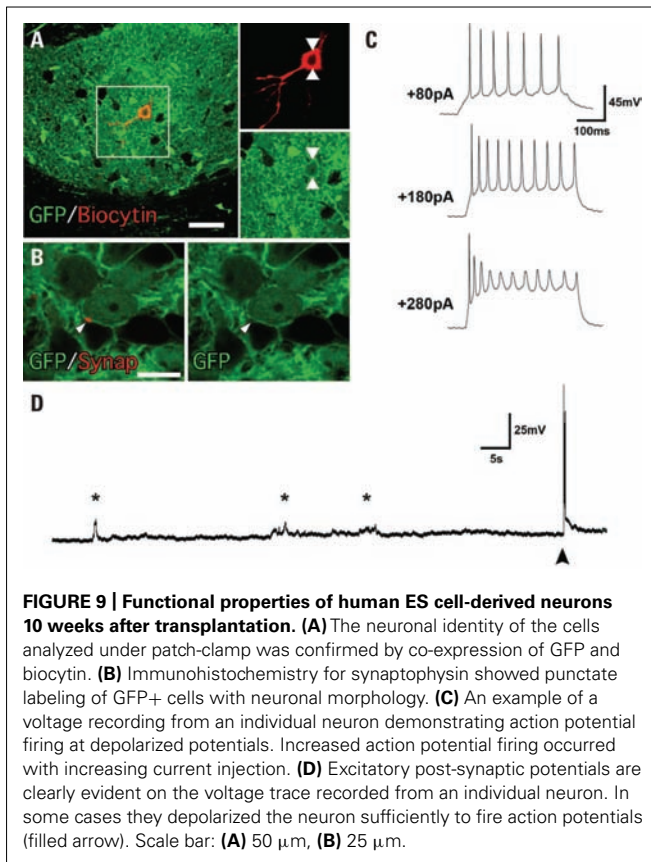 photo-montage shows a GFP+ graft placed in the ventral striatum adjacent to the corpus callosum adjacent to numerous host RIP+ fiber bundles. **(C–E)** GFP+ fibers closely follow the trajectory of RIP+ white matter tracts. **(F–H)** Many GFP+ fibers were also found coursing through the anterior commissure. Scale bar: **(A)** 200 μm, **(C–H)**, 50 μm.

the grafts suggests significant growth through cell division after transplantation and the presence of Ki67+/Sox2+ cells showed a persistence of some level of neural growth at the 10-week survival time. Given the protracted growth properties of human cells this is comparable with previously observed growth properties of fetal tissue grafts after transplantation, which can expand in volume five- to eightfold in the first 2 weeks after grafting (Labandeira-Garcia et al., 1991). Although there are well-recognized safety concerns related to tumor formation from uncontrolled proliferation of pluripotent cell-derived preparations *in vivo* (Morizane et al., 2006; Roy et al., 2006), we did not observe any overt signs of tumor formation at the gross morphology level. Distinguishing between normal developmental growth and pathological growth properties (perhaps with slow but persistent growth kinetics) will require additional studies with significantly longer survival times.

The presence of doublecortin+ and PSA-NCAM+ cells migrating from the graft into the adjacent host parenchyma indicates on-going neurogenesis as part of the dynamic growth properties of the grafts at 10 weeks. Importantly, the grafts also contained differentiated neurons and glia, with the neuronal component representing more than half of the transplanted cells (at least based on immunolabeling for NeuN, which may in fact underestimate the total neuron numbers assuming not all express NeuN). Based on the average cell densities and graft volumes, this equates to a density of approximately 1.4×10^5 neurons/mm^3. For transplantation-based approaches for brain repair, the numbers of a therapeutic cell type as a function of graft volume is important to consider. The cell numbers should be sufficient to achieve the desired functional effect, while maintaining a graft size that does not damage host nuclei at the site of implantation. In this context, the present results compare favorably to those from grafting of ventral mesencephalic tissue into the forebrain of patients

with PD. Recent post-mortem results from two patients with well-defined clinical benefit up to 3 years after grafting showed that the density of therapeutic dopamine neurons at each graft site was in the order of 0.2 to 2.4×10^3 dopamine neurons/mm^3 (Mendez et al., 2005).

We cannot assume, however, a uniform composition of neuronal phenotypes in the ES cell-derived grafts. Our results showed a heterogeneous distribution of neuronal subtypes at both the morphological and molecular level. The cytoplasmic distribution of GFP allowed for detailed analysis of cell morphology and revealed a variety of mature neuronal profiles including those with bipolar, pyramidal, and stellate morphology. Similarly, the heterogeneous distribution of Ctip2+ cells within the grafts highlights the mixed neuronal composition. The Ctip2+ fractions appeared in localized clusters, suggesting some level of regional organization within the grafts. The appearance of Ctip2 expression in the grafts may identify cells representing deep-layer cortical projection neurons. This would be in line with the *in vitro* results, which showed some differentiated neural precursors expressed markers consistent with dorsal forebrain identity, including Pax7 and Otx2 and also with recent studies demonstrating the default propensity of both mouse and human ES cells to adopt cortical fates after neural induction when differentiated under minimalist conditions (Watanabe et al., 2005; Eiraku et al., 2008; Gaspard et al., 2008). The absence of other markers of cortical projection neuron identity, such as Cux1 and Tbr1, may reflect that not all cortical subtypes are generated under the differentiation conditions we have used here. Indeed, previous studies have shown that the temporal staging of cortical layer specification during normal corticogenesis is recapitulated *in vitro* as a function of differentiation time (Eiraku et al., 2008; Gaspard et al., 2008; Koch et al., 2009; Shi et al., 2012). In the present study, the relatively short differentiation

FIGURE 9 | Functional properties of human ES cell-derived neurons 10 weeks after transplantation. (A) The neuronal identity of the cells analyzed under patch-clamp was confirmed by co-expression of GFP and biocytin. **(B)** Immunohistochemistry for synaptophysin showed punctate labeling of GFP+ cells with neuronal morphology. **(C)** An example of a voltage recording from an individual neuron demonstrating action potential firing at depolarized potentials. Increased action potential firing occurred with increasing current injection. **(D)** Excitatory post-synaptic potentials are clearly evident on the voltage trace recorded from an individual neuron. In some cases they depolarized the neuron sufficiently to fire action potentials (filled arrow). Scale bar: **(A)** 50 μm, **(B)** 25 μm.

time *in vitro* and maturation time *in vivo* may favor the production of earlier born, Ctip2+, deep-layer cortical phenotypes rather than later born, Cux1+ neurons that populate superficial layers during normal development.

The use of neonatal recipients in neural transplantation studies offers unique insight into the intrinsic growth properties of transplanted neurons by offering a relatively growth-permissive compared to the more inhibitory environment of the adult brain (Abrous et al., 1993; Olsson et al., 1997; Bentlage et al., 1999; Thompson et al., 2005, 2008). Here we have described in detail the remarkable intrinsic capacity of neurons derived from human ES cells for extensive growth *in vivo* after transplantation. A conspicuous feature of the neuronal growth properties was the association of long-distance GFP+ fiber growth with major white matter pathways in the host brain including: forceps minor, anterior commissure, with extensive growth rostrally along the rostro-caudal axis through forceps minor, and caudally along fasciculus retroflexus and striatal fiber bundles of the internal capsule, continuing through the cerebral peduncle into the brain stem; and also along the medio-lateral axis throughout the anterior commissure and corpus callosum, where GFP+ fibers extended into the overlying cortex in both hemispheres. This finding is consistent throughout an extensive body of work using various donor materials combined with different host species, age, and graft location (Wictorin et al., 1990; Isacson et al., 1995; Isacson and Deacon, 1996; Englund et al., 2002; Baker and Mendez, 2005; Gaillard et al., 2007; Thompson et al., 2008; Nasonkin et al.,

2009; Hargus et al., 2010; Ideguchi et al., 2010; Steinbeck et al., 2012), and supports the idea that white matter associated fiber outgrowth may be a generalized feature mediated by the host environment.

It leads us to speculate that relatively undifferentiated cells may take their growth and guidance cues from the host environment in place of any intrinsically specified programs for target-directed connectivity. Conversely, cells with a certain threshold level of intrinsic specification will have an over-riding ability to innervate specific targets independently of white matter associated growth cues. In support of this, we have previously shown that specific dopamine subtypes in intra-striatal grafts of ventral mesencephalon (VM) are intrinsically programmed to innervate their normal developmental targets at the time of implantation (Thompson et al., 2005; Grealish et al., 2010). Notably, however, intra-striatal VM grafts also send long-distance projections along the internal capsule and into the host midbrain in order to form a pathway that does not match with any of the known intrinsic projection patterns originating from the midbrain itself in the adult brain (Isacson and Deacon, 1996; Thompson et al., 2008). Thus, the overall pattern of growth may reflect both target-oriented growth from intrinsically specified progenitors, including those for dopamine neurons, as well as growth directed by signals from host white matter compartments acting on partially/undifferentiated cells contained in fetal tissue preparations.

Differentiating between these two possible growth mechanisms becomes difficult when examining axonal patterns from grafts expected to contain neurons that normally form part of, or course through, white matter tracts – such as cortical projection neurons. At least one study using fetal cortical donor tissue from a GFP reporter mouse has shown convincingly that in addition to growth along white matter tracts, grafted cortical neurons extensively innervate the contralateral cortical gray matter as well as appropriate subcortical targets, including the striatum and thalamus (Gaillard et al., 2007). On the other hand, studies using stem cell-derived donor material, including the present work, appear to show growth throughout the internal and external capsules as the predominate feature (Ideguchi et al., 2010; Steinbeck et al., 2012) without extensive patterns of terminal arborization in expected cortical target areas. In the present study, we cannot discount that this may be due to a relatively immature state of the grafts at 10 weeks. The expression of molecular markers of cortical projection phenotype, such as Ctip2, support the interpretation that at least some component of the graft-derived outgrowth originates from cortical neurons displaying appropriate, target-directed growth features. These results highlights an on-going need to rigorously assess the ability of stem cell-derived neurons to innervate specific targets after transplantation. Further studies with longer survival times and also various differentiation procedures aimed at generating cortical progenitors with different laminar identities will be important for determining the capacity for specific cortical phenotypes to innervate appropriate targets after transplantation. Functional circuit replacement for brain repair will more than likely require that transplanted neurons can functionally innervate denervated targets.

In addition to facilitating a detailed analysis of anatomical graft features the GFP reporter allowed us to assess functional aspects of graft integration through patch-clamp experiments. The results showed that, despite the relatively early survival time, the grafts contained differentiated neurons capable of firing action potentials with stereotypical neuronal behavior, including increased frequency of action potential firing in response to increasing current injection. This is in line with recent findings showing human ES cell-derived neurons with mature electrophysiological profiles following transplantation into the telencephalon of neonatal SCID mice (Koch et al., 2009). We also observed that at resting membrane potential the grafted neurons exhibited excitatory postsynaptic potentials and spontaneous action potentials, suggesting functional afferent input. In support of this, many of the grafted cells showed punctate labeling for synaptophysin, including examples of synaptophysin+/GFP− patterns, suggesting the possibility of host-specific afferent input. Further studies will be required to distinguish between the relative contribution from graft and host afferent input to grafted neurons and also the ability of grafted neurons to functionally activate host neurons.

In summary, we report here that neurons generated from human ES cells are capable of extensive growth within the host brain after intra-cerebral transplantation and display properties consistent with functional integration at the electrophysiological level. These are encouraging findings in the context of current efforts to establish stem cell-based procedures for brain repair. Certain features of the grafts, including the patterns of fiber outgrowth and expression of Ctip2, support recent findings describing the efficient procurement of cortical neurons from human ES cells. Using stem cells to replace cortical circuitry may lead to improved treatments for cortical injury, for example following acute damage arising from trauma or stroke, or as part of neurodegenerative processes associated with motor neuron disease or Huntington's disease. A significant challenge will be to generate cell preparations that give rise to neurons capable of long-range re-instatement of specific, and potentially multiple cortical pathways (e.g., corresponding to distinct laminar identities), based on an intrinsic capacity for functional innervation of appropriate targets. This will require extensive growth within the host brain as well as target-directed axonal guidance. Our results show that transplanted neurons derived from human ES cells have an impressive intrinsic capacity for long-distance axonal growth *in vivo*, while evidence for target-specific innervation and terminal ramification in expected cortical target nuclei was more limited. Further studies on the connectivity of stem cell-derived neurons after transplantation will form a critical part of the basic research required for translation of recent advances in pluripotent stem cell biology to effective procedures for brain repair.

REFERENCES

Abrous, D. N., Torres, E. M., and Dunnett, S. B. (1993). Dopaminergic grafts implanted into the neonatal or adult striatum: comparative effects on rotation and paw reaching deficits induced by subsequent unilateral nigrostriatal lesions in adulthood. *Neuroscience* 54, 657–668.

Baker, K. A., and Mendez, I. (2005). Long distance selective fiber outgrowth of transplanted hNT neurons in white matter tracts of the adult rat brain. *J. Comp. Neurol.* 486, 318–330.

Barberi, T., Klivenyi, P., Calingasan, N. Y., Lee, H., Kawamata, H., Loonam, K., Perrier, A. L., Bruses, J., Rubio, M. E., Topf, N., Tabar, V., Harrison, N. L., Beal, M. F., Moore, M. A., and Studer, L. (2003). Neural subtype specification of fertilization and nuclear transfer embryonic stem cells and application in parkinsonian mice. *Nat. Biotechnol.* 21, 1200–1207.

Bentlage, C., Nikkhah, G., Cunningham, M. G., and Bjorklund, A. (1999). Reformation of the nigrostriatal pathway by fetal dopaminergic micrografts into the substantia nigra is critically dependent on the age of the host. *Exp. Neurol.* 159, 177–190.

Cavalieri, B. (1966). *Geometric degl: Indivisible.* Turin: Unione Tipografico, Editrice.

Chambers, S. M., Fasano, C. A., Papapetrou, E. P., Tomishima, M., Sadelain, M., and Studer, L. (2009). Highly efficient neural conversion of human ES and iPS cells by dual inhibition of SMAD signaling. *Nat. Biotechnol.* 27, 275–280.

Conley, B. J., Denham, M., Gulluyan, L., Olsson, F., Cole, T. J., and Mollard, R. (2005). Mouse embryonic stem cell derivation, and mouse and human embryonic stem cell culture and differentiation as embryoid bodies. *Curr. Protoc. Cell Biol.* Chapter 23, Unit 23.2.

Costa, M., Dottori, M., Ng, E., Hawes, S. M., Sourris, K., Jamshidi, P., Pera, M. F., Elefanty, A. G., and Stanley, E. G. (2005). The hESC line Envy expresses high levels of GFP in all differentiated progeny. *Nat. Methods* 2, 259–260.

Dottori, M., and Pera, M. F. (2008). Neural differentiation of human embryonic stem cells. *Methods Mol. Biol.* 438, 19–30.

Eiraku, M., Watanabe, K., Matsuo-Takasaki, M., Kawada, M., Yonemura, S., Matsumura, M., Wataya, T., Nishiyama, A., Muguruma, K., and Sasai, Y. (2008). Self-organized formation of polarized cortical tissues from ESCs and its active manipulation by extrinsic signals. *Cell Stem cell* 3, 519–532.

Englund, U., Fricker-Gates, R. A., Lundberg, C., Bjorklund, A., and Wictorin, K. (2002). Transplantation of human neural progenitor cells into the neonatal rat brain: extensive migration and differentiation with long-distance axonal projections. *Exp. Neurol.* 173, 1–21.

Gaillard, A., and Jaber, M. (2011). Rewiring the brain with cell transplantation in Parkinson's disease. *Trends Neurosci.* 34, 124–133.

Gaillard, A., Prestoz, L., Dumartin, B., Cantereau, A., Morel, F., Roger, M., and Jaber, M. (2007). Reestablishment of damaged adult motor pathways by grafted embryonic cortical neurons. *Nat. Neurosci.* 10, 1294–1299.

Gaspard, N., Bouschet, T., Hourez, R., Dimidschstein, J., Naeije, G., Van Den Ameele, J., Espuny-Camacho, I., Herpoel, A., Passante, L., Schiffmann, S. N., Gaillard, A., and Vanderhaeghen, P. (2008). An intrinsic mechanism of corticogenesis from embryonic stem cells. *Nature* 455, 351–357.

Grealish, S., Jonsson, M. E., Li, M., Kirik, D., Bjorklund, A., and Thompson, L. H. (2010). The A9 dopamine neuron component in grafts of ventral mesencephalon is an important determinant for recovery of motor function in a rat model of Parkinson's disease. *Brain* 133, 482–495.

Hargus, G., Cooper, O., Deleidi, M., Levy, A., Lee, K., Marlow, E., Yow, A., Soldner, F., Hockemeyer, D., Hallett, P. J., Osborn, T., Jaenisch, R., and Isacson, O. (2010). Differentiated Parkinson patient-derived induced pluripotent stem cells grow

in the adult rodent brain and reduce motor asymmetry in Parkinsonian rats. *Proc. Natl. Acad. Sci. U.S.A.* 107, 15921–15926.

Ideguchi, M., Palmer, T. D., Recht, L. D., and Weimann, J. M. (2010). Murine embryonic stem cell-derived pyramidal neurons integrate into the cerebral cortex and appropriately project axons to subcortical targets. *J. Neurosci.* 30, 894–904.

Isacson, O., and Deacon, T. W. (1996). Specific axon guidance factors persist in the adult brain as demonstrated by pig neuroblasts transplanted to the rat. *Neuroscience* 75, 827–837.

Isacson, O., Deacon, T. W., Pakzaban, P., Galpern, W. R., Dinsmore, J., and Burns, L. H. (1995). Transplanted xenogeneic neural cells in neurodegenerative disease models exhibit remarkable axonal target specificity and distinct growth patterns of glial and axonal fibres. *Nat. Med.* 1, 1189–1194.

Koch, P., Opitz, T., Steinbeck, J. A., Ladewig, J., and Brustle, O. (2009). A rosette-type, self-renewing human ES cell-derived neural stem cell with potential for in vitro instruction and synaptic integration. *Proc. Natl. Acad. Sci. U.S.A.* 106, 3225–3230.

Labandeira-Garcia, J. L., Wictorin, K., Cunningham, E. T. Jr., and Bjorklund, A. (1991). Development of intrastriatal striatal grafts and their afferent innervation from the host. *Neuroscience* 42, 407–426.

Li, W., Sun, W., Zhang, Y., Wei, W., Ambasudhan, R., Xia, P., Talantova, M., Lin, T., Kim, J., Wang, X., Kim, W. R., Lipton, S. A., Zhang, K., and Ding, S. (2011). Rapid induction and long-term self-renewal of primitive neural precursors from human embryonic stem cells by small molecule inhibitors. *Proc. Natl. Acad. Sci. U.S.A.* 108, 8299–8304.

Lindvall, O., and Bjorklund, A. (2004). Cell therapy in Parkinson's disease. *NeuroRx* 1, 382–393.

Lindvall, O., and Hagell, P. (2000). Clinical observations after neural transplantation in Parkinson's disease. *Prog. Brain Res.* 127, 299–320.

Mendez, I., Sanchez-Pernaute, R., Cooper, O., Vinuela, A., Ferrari, D., Bjorklund, L., Dagher, A., and Isacson, O. (2005). Cell type analysis of functional fetal dopamine cell suspension transplants in the striatum and substantia nigra of patients with Parkinson's disease. *Brain* 128, 1498–1510.

Morizane, A., Doi, D., Kikuchi, T., Nishimura, K., and Takahashi, J. (2011). Small-molecule inhibitors of bone morphogenic protein and activin/nodal signals promote highly efficient neural induction from human pluripotent stem cells. *J. Neurosci. Res.* 89, 117–126.

Morizane, A., Takahashi, J., Shinoyama, M., Ideguchi, M., Takagi, Y., Fukuda, H., Koyanagi, M., Sasai, Y., and Hashimoto, N. (2006). Generation of graftable dopaminergic neuron progenitors from mouse ES cells by a combination of coculture and neurosphere methods. *J. Neurosci. Res.* 83, 1015–1027.

Nasonkin, I., Mahairaki, V., Xu, L., Hatfield, G., Cummings, B. J., Eberhart, C., Ryugo, D. K., Maric, D., Bar, E., and Koliatsos, V. E. (2009). Long-term, stable differentiation of human embryonic stem cell-derived neural precursors grafted into the adult mammalian neostriatum. *Stem Cells* 27, 2414–2426.

Nikkhah, G., Winkler, C., Rödter, A., and Samii, M. (2000). "Microtransplantation of nigral dopamine neurons: a "step by step" recipe.," in *Neuromethods: Cell and Tissue Transplantation in the CNS*, eds. S. B. Dunnett, A. A. Boulton, and G. B. Baker (Totowa: The Human Press), 207–231.

Olsson, M., Bentlage, C., Wictorin, K., Campbell, K., and Bjorklund, A. (1997). Extensive migration and target innervation by striatal precursors after grafting into the neonatal striatum. *Neuroscience* 79, 57–78.

Pera, M. F., Andrade, J., Houssami, S., Reubinoff, B., Trounson, A., Stanley, E. G., Ward-Van Oostwaard, D., and Mummery, C. (2004). Regulation of human embryonic stem cell differentiation by BMP-2 and its antagonist noggin. *J. Cell Sci.* 117, 1269–1280.

Perrier, A. L., Tabar, V., Barberi, T., Rubio, M. E., Bruses, J., Topf, N., Harrison, N. L., and Studer, L. (2004). Derivation of midbrain dopamine neurons from human embryonic stem cells. *Proc. Natl. Acad. Sci. U.S.A.* 101, 12543–12548.

Reubinoff, B. E., Itsykson, P., Turetsky, T., Pera, M. F., Reinhartz, E., Itzik, A., and Ben-Hur, T. (2001). Neural progenitors from human embryonic stem cells. *Nat. Biotechnol.* 19, 1134–1140.

Reubinoff, B. E., Pera, M. F., Fong, C. Y., Trounson, A., and Bongso, A. (2000). Embryonic stem cell lines from human blastocysts: somatic differentiation in vitro. *Nat. Biotechnol.* 18, 399–404.

Roy, N. S., Cleren, C., Singh, S. K., Yang, L., Beal, M. F., and Goldman, S. A. (2006). Functional engraftment of human ES cell-derived dopaminergic neurons enriched by coculture with telomerase-immortalized midbrain astrocytes. *Nat. Med.* 12, 1259–1268.

Shi, Y., Kirwan, P., Smith, J., Robinson, H. P., and Livesey, F. J. (2012). Human cerebral cortex development from pluripotent stem cells to functional excitatory synapses. *Nat. Neurosci.* 15, 477–486.

Sonntag, K. C., Pruszak, J., Yoshizaki, T., Van Arensbergen, J., Sanchez-Pernaute, R., and Isacson, O. (2007). Enhanced yield of neuroepithelial precursors and midbrain-like dopaminergic neurons from human embryonic stem cells using the bone morphogenic protein antagonist noggin. *Stem Cells* 25, 411–418.

Steinbeck, J. A., Koch, P., Derouiche, A., and Brustle, O. (2012). Human embryonic stem cell-derived neurons establish region-specific, long-range projections in the adult brain. *Cell. Mol. Life Sci.* 69, 461–470.

Tabar, V., Panagiotakos, G., Greenberg, E. D., Chan, B. K., Sadelain, M., Gutin, P. H., and Studer, L. (2005). Migration and differentiation of neural precursors derived from human embryonic stem cells in the rat brain. *Nat. Biotechnol.* 23, 601–606.

Thompson, L., Barraud, P., Andersson, E., Kirik, D., and Bjorklund, A. (2005). Identification of dopaminergic neurons of nigral and ventral tegmental area subtypes in grafts of fetal ventral mesencephalon based on cell morphology, protein expression, and efferent projections. *J. Neurosci.* 25, 6467–6477.

Thompson, L. H., Grealish, S., Kirik, D., and Bjorklund, A. (2009). Reconstruction of the nigrostriatal dopamine pathway in the adult mouse brain. *Eur. J. Neurosci.* 30, 625–638.

Thompson, L. H., Kirik, D., and Bjorklund, A. (2008). Non-dopaminergic neurons in ventral mesencephalic transplants make widespread axonal connections in the host brain. *Exp. Neurol.* 213, 220–228.

Watanabe, K., Kamiya, D., Nishiyama, A., Katayama, T., Nozaki, S., Kawasaki, H., Watanabe, Y., Mizuseki, K., and Sasai, Y. (2005). Directed differentiation of telencephalic precursors from embryonic stem cells. *Nat. Neurosci.* 8, 288–296.

Wictorin, K., Brundin, P., Gustavii, B., Lindvall, O., and Bjorklund, A. (1990). Reformation of long axon pathways in adult rat central nervous system by human forebrain neuroblasts. *Nature* 347, 556–558.